RoboX: An End-to-End Solution to Accelerate Autonomous Control in Robotics

Jacob Sacks   Divya Mahajan   Richard C. Lawson   Hadi Esmaeilzadeh[†]

Alternative **C**omputing **T**echnologies (**ACT**) Lab

Georgia Institute of Technology
{jsacks, divya_mahajan, rlawson}@gatech.edu

[†]University of California, San Diego
hadi@eng.ucsd.edu

Abstract—Novel algorithmic advances have paved the way for robotics to transform the dynamics of many social and enterprise applications. To achieve true autonomy, robots need to continuously process and interact with their environment through computationally-intensive motion planning and control algorithms under a low power budget. Specialized architectures offer a potent choice to provide low-power, high-performance accelerators for these algorithms. Instead of taking a traditional route which profiles and maps hot code regions to accelerators, this paper delves into the algorithmic characteristics of the application domain. We observe that many motion planning and control algorithms are formulated as a constrained optimization problems solved online through Model Predictive Control (MPC). While models and objective functions differ between robotic systems and tasks, the structure of the optimization problem and solver remain fixed. Using this theoretical insight, we create *RoboX*, an end-to-end solution which exposes a high-level domain-specific language to roboticists. This interface allows roboticists to express the physics of the robot and its task in a form close to its concise mathematical expressions. The *RoboX* backend then automatically maps this high-level specification to a novel programmable architecture, which harbors a programmable memory access engine and compute-enabled interconnects. Hops in the interconnect are augmented with simple functional units that either operate on in-fight data or are bypassed according a micro-program. Evaluations with six different robotic systems and tasks show that *RoboX* provides a 29.4× (7.3 ×) speedup and 22.1× (79.4×) performance-per-watt improvement over an ARM Cortex A57 (Intel Xeon E3). Compared to GPUs, *RoboX* attains 7.8×, 65.5×, and 71.8× higher Performance-per-Watt to Tegra X2, GTX 650 Ti, and Tesla K40 with a power envelope of only 3.4 Watts at 45 nm.

Keywords-Accelerators; domain-specific languages; DSL; in-network computing; model predictive control; MPC; robotics

I. Introduction

Advances in robotics have had a revolutionary impact on many diverse sectors, ranging from space exploration [1] to medicine [2] to manufacturing [3]. Although robots are set to transform many enterprise sectors, enabling true autonomy and adaptation is predicated on compute-intensive motion planning and control algorithms. Adding improved compute capabilities using general-purpose platforms often requires larger batteries or shortening of the robot's operational time. Higher capacity batteries increases the weight and/or form factor, which often does not comply with the application requirements [4]. Under these constraints, only a relatively small portion of battery capacity (power) can be allocated to compute resources. In other words, a robot is required to perform copious amount of computation in disproportionately small power envelopes. This discrepancy is more pronounced in smaller systems (e.g., micro/pico Unmanned Aerial Vehicles (UAVs)), which are increasingly gaining traction for use in retail assistance, home care, photography, and surveillance applications.

For instance, a popular consumer UAV, the DJI Phantom 2 [5], requires roughly 131.4 W to power its motors for 25 minutes, its maximum flight time. The exorbitant power consumption of the motors requires all other electronics and peripherals, including the camera, to operate under a restricted power budget of approximately 5.6 W. Such constraints limit the capabilities of the Phantom 2, as complex, autonomous maneuvers require more compute-intensive algorithms operating at greater control frequencies [6]. Providing such abilities with general-purpose hardware would be prohibitively more power-hungry and curtail the already short flight time. Furthermore, as the robot size decreases, the compute power dissipation can become comparable to that of its actuators [4,7]–[10]. These unique challenges call for innovative techniques that offer greater compute capabilities under constrained power budgets.This paper sets out to devise such a solution through hardware acceleration for motion planning and control. Another complementary alternative is to offload most of the computation to off-board local servers or remote clouds. Nonetheless, our hardware accelerator can be utilized to augment the servers and/or reduce their power consumption. Although our solution is agnostic to offloading, it opens the door for motion planning and control on the edge. Computation on the edge is specifically attractive for robotic applications such as disaster rescue missions with intermittent connectivity or military operations where continuous communication with the base station can compromise the stealth capabilities of the robot.

Recent works have focused extensively on acceleration for machine learning [11]–[19]; however, this work instead emphasizes robot motion planning and control. We aim to move beyond the traditional practices of acceleration, which rely heavily on identifying and mapping compute intensive kernels from existing libraries and applications to specialized hardware. Instead, we provide an end-to-end solution, named *RoboX*[1] , that enables roboticists to express the physics of the robot and its task in a novel high-level mathematical domain-specific language (DSL). In devising *RoboX*, we adopt roboticists' general approach of describing the robot's physical dynamics as a series of time-varying states, control inputs, and physical constraints. The robotic task is then expressed as a constrained optimization problem. Solving this problem outputs the trajectory of the control inputs and state variables over a discrete number of future time steps. However, pre-solving this problem once before execution does not account for environmental events. Therefore, the optimization problem is continuously solved *online*. A commonly used framework is Model Predictive Control (MPC) [6,20]–[29], which uses a mathematical model of the robot to predictively plan its behavior over a finite time horizon. As such, MPC is capable of anticipating future events whilst taking into consideration realistic constraints of the robot to plan its current action. A key insight is that while the robot models and task expressions differ across robotic systems and applications, the general structure of the MPC formulation is effectively invariant. *RoboX*'s DSL exploits this insight to provide high-level language constructs that enable modeling and expression of robotic applications close to roboticists intuition. The *RoboX* compiler then automatically maps this high-level specification to a novel programmable accelerator and alleviates the burden of programming the accelerator with low-level primitives and APIs.

---

[1]*RoboX* is phonetically pronounced "ro · box."

As such the paper makes the following contributions.

1) To move beyond conventional approaches of profiling and partially mapping code regions to specialized hardware modules, we build our acceleration solution atop an algorithmic understanding of the application domain. We observe that many diverse robotic applications are formulated as constrained optimization problems which can be solved online using Model Predictive Control. Using this insight, we develop *RoboX*, an end-to-end acceleration solution for robotic motion planning and control.

2) *RoboX* encapsulates a domain-specific language which enables programmers to express robotic applications close to their concise mathematical description. We provide a compiler which transforms this high-level specification into a concrete MPC formulation and solver, which is mapped to the accelerator.

3) The *RoboX* architecture introduces compute-enabled on-chip interconnections, where hops integrate simple functional units. This functional unit, if required, can perform operations on in-transit data to reduce the burden on compute units. To support this architecture, we devise an ISA that offers three categories of instructions, where each program the interconnect, compute units, and memory interface, respectively. This flexibility allows efficiently executing different phases of robotic applications that alternate between dynamics and solver computation.

Using cycle-accurate simulations, we evaluate *RoboX* over six different robots: mobile robot, autonomous vehicle, manipulator, micro-satellite, quadrotor, and hexacopter. We compare *RoboX* to an optimized CPU implementation on a Intel Xeon E3 and ARM Cortex A57 and a custom GPU implementation on a Tegra X2, GTX 650 Ti, and Tesla K40. On average, *RoboX*, under a power budget of 3.4 Watts at 45 nm, provides $29.4\times$ ($7.3\times$) speedup over ARM A57 (Xeon E3) and a $7.8\times$, $65.5\times$, and $71.8\times$ average performance-per-watt improvement compared to the Tegra X2, GTX 650 Ti, and Tesla K40, respectively. Results suggest that *RoboX* marks a first step towards enabling comprehensive solutions for robotic acceleration from high-level mathematical specifications.

II. MOTION PLANNING AND CONTROL

Before delving into the details of *RoboX*, we provide a background on robotic modeling and control. Below, we describe the details of the system models and the formulation of the constrained optimization problems solved online with MPC.

A. System Modeling and Dynamics

Models of complex robotic systems generally consist of a set of system states, control inputs, and system dynamics. In Figure 1a, we illustrate an example of a quadrotor, which has states corresponding to its Cartesian coordinates (x, y, z) in a fixed inertial frame. States corresponding to its orientation in terms of yaw (ϕ), pitch (θ), and roll (ψ) are also shown. The illustration depicts the quadrotor's control inputs, i.e., each rotor's generated thrust (f_1, f_2, f_3, f_4). A robot model then provides a description of how these states and inputs influence each other over time through a set of differential equations known as the system dynamics. The canonical form of general nonlinear dynamics is given as:

$$\dot{x} = f(x, u) \qquad (1)$$

where x and u constitute robot's states and control inputs, respectively. The function $f(\cdot, \cdot)$ is a vector-valued generic nonlinear function of current states and control inputs, and $\dot{x}$ is a time derivative of
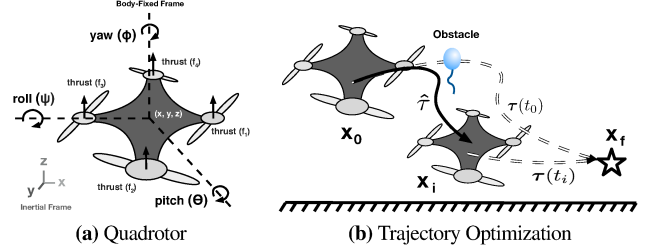

(a) Quadrotor **(b)** Trajectory Optimization

Figure 1: (a) States and control inputs of a quadrotor. **(b)** Quadrotor planning trajectory $\tau(t_0)$ towards target (star) and adjusting course to $\hat{\tau}$ due to obstacle (balloon), while staying above altitude $\underline{z}$ due to a constraint.

x $(\partial x / \partial t)$. For the quadrotor example, we can express its velocity as:

$$\dot{z} = g - \frac{b}{m} \cos\phi \, \cos\theta \, f_T \qquad (2)$$

where b, m, and g are constants, and $f_T = \sum_{i=1}^{4} f_i^2$ is the total thrust. These models also incorporate the robot's physical constraints. In this case, the propellers' generated thrust has limits, and the quadrotor's orientation must stay within a reasonable range to avoid flipping over. Such constraints are expressed as inequalities over states/control inputs in the optimization problem. Next, we need to define how to formulate the optimization problem for a desired task.

B. Model Predictive Control

Model Predictive Control solves a constrained optimization problem online at every time step to plan and refine the trajectory of the robot. For example, in Figure 1b, we show a quadrotor at its initial state x_0 with an objective of reaching target state x_f, the star. The MPC problem converges to an optimal trajectory $\tau(t_0)$, and the controller then applies the first control decision to the quadrotor. Since the problem is solved online, the trajectory can be continuously refined to adapt to environmental changes. In this example, an obstacle, i.e., a balloon appears, and the quadrotor changes course accordingly. The actual path taken by the quadrotor, $\hat{\tau}$, is now different than one initially planned.

The robot's task is specified as an objective function minimized over a number of future times steps, called the prediction horizon. Longer horizons can improve convergence and lead to more robust control in reaction to external disturbances and obstacles. For the quadrotor, the goals of reaching the target while avoiding the obstacle are incorporated as separate terms in the objective function:

$$J = P_{tr}(x(t_f), Q_{tr}) + \int_{t_0}^{t_f} P_{ob}(x(t), Q_{ob}) dt \qquad (3)$$

where $P_{tr}(\cdot)$ penalizes distance from the target, $P_{ob}(\cdot)$ penalizes proximity to an obstacle, and Q_{tr} and Q_{ob} are weights which indicate the relative importance of each penalty. Penalties incorporated in the objective can be categorized as either running cost or terminal cost. The penalty for obstacle avoidance, $P_{ob}(\cdot)$, is the running cost, as it is enforced at every point along the horizon except at the final point t_f. The penalty corresponding to reaching the target is the terminal cost, as it solely considers the final state $x(t_f)$. The final constrained optimization problem then becomes:

$$\min_{x(\cdot), \, u(\cdot)} J(x(\cdot), u(\cdot))$$
$$s.t. \; x(0) = x_0,$$
$$\dot{x} = f(x(t), u(t)), \, \forall t \in [0, t_f] \qquad (4)$$
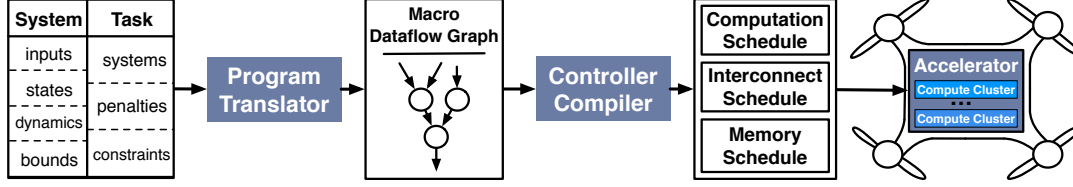$$\underline{u} \leq u(t) \leq \bar{u}, \, \forall t \in [0, t_f]$$

Figure 2: *RoboX* constitutes a domain-specific language, a unique hardware accelerator, and an automated compilation workflow.

where $x(t)$, $u(t)$ are the states and inputs at time t, $f(\cdot,\cdot)$ is the quadrotor's dynamics, and x_0 is the current state. We have placed constraints $\underline{u}$, $\bar{u}$ on the control input u, which correspond to the physical limitations of the propellers. This formulation of the constrained optimization problem in Equation 4 is entirely independent of the solver.

As its solver, *RoboX* uses the primal-dual interior point method [30]. We chose this method as it is commonly used in constrained robotics applications [31]–[36]. This method first discretizes the trajectory over a horizon of length N:

$$z = \begin{bmatrix} x_0^T & ... & x_N^T & u_0^T & ... & u_{N-1}^T \end{bmatrix}^T \quad (5)$$

where x_i and u_i are state and input vectors at each discrete time point i. Then, all the equality constraints corresponding to the quadrotor's current position and dynamics are concatenated along the horizon into a vector g. Similarly, we construct a vector h which contains all inequality constraints corresponding to the bounds on the propeller thrusts along the horizon. Instead of directly solving for the states and inputs of the trajectory, interior point methods solve for updates Δz to the current estimates. This solution is found by solving the sparse linear system of the form:

$$\begin{bmatrix} H & g_{\Delta z}^T & h_{\Delta z}^T & \\ g_{\Delta z} & & & \\ h_{\Delta z} & & I & \\ & & S & \Lambda \end{bmatrix} \begin{bmatrix} \Delta z \\ \Delta \mu \\ \Delta \lambda \\ \Delta s \end{bmatrix} = - \begin{bmatrix} J_{\Delta z} \\ g \\ h \\ S\Lambda \end{bmatrix} \quad (6)$$

where $J_{\Delta z}$ and H are gradient and Hessian of the objective function, and $g_{\Delta z}$ and $h_{\Delta z}$ are gradients of the constraints. The variables $\Delta \lambda$, $\Delta \mu$, and Δs are updates to special variables, known as KKT multipliers and slack variables, used by the interior point method to account for constraints. The matrices S, Λ, I are $diag(s)$, $diag(\lambda)$, and the identity matrix, respectively. *RoboX* uses a combination of Cholesky decomposition [35] and forward/backward substitution [37] to solve the linear system in Equation 6. The solution provides updates, Δz, which are applied to the current trajectory. This process is repeated until convergence, after which the control decisions are supplied to the quadrotor.

The algorithms described above provide the theoretical foundation for *RoboX* to target a wide range of robotic applications. A roboticist simply provides a high-level description of the physics and constraints of the robot and a mathematical expression of its objective. The backend of *RoboX* then translates this high-level specification into the corresponding constrained optimization problem and generates the concrete Interior Point Method solver.

III. ROBOX WORKFLOW

RoboX aims to enable roboticists to benefit from acceleration without departing from their concise mathematical formulations. Using these expressions, *RoboX* automatically generates the optimization problem and solver and compiles it into static schedules for the accelerator. We discuss each component shown in Figure 2.

DSL for planning and control. The goal of *RoboX*'s programming interface is to stay close to the concise mathematical descriptions intuitive for roboticists. It is a high-level DSL which distills MPC problems into distinct components: (1) a robot component which enumerates robot's inputs and states, its dynamics, and any input/state constraints and (2) a task component to provide penalty terms and constraints specific to the robot's goal. Lastly, the programmer provides meta-parameters, such as prediction horizon length, desired controller rate, and convergence criteria.

Program translator and controller compiler. From the DSL specification of the robot and its task, *RoboX*'s *Program Translator* assigns an ordering to all states, inputs, penalty terms, and constraints. Using this ordering, the Program Translator generates a macro dataflow graph (M-DFG) of the control algorithm. Next, the *Controller Compiler* takes this M-DFG and generates a static schedule for the computation, interconnect, and programmable memory access engine. *RoboX* provides a novel ISA, which enables programmability for each of these architectural components while abstracting away hardware implementation details.

Accelerator architecture with compute-enabled interconnect. The *RoboX* architecture is organized as a hierarchical cluster of compute units. Each compute unit within a cluster can execute independent operations on different data or function together as a SIMD unit. The novel compute-enabled interconnect enables light-weight computation to be performed on in-transit data. This innovation is imperative for the design of our accelerator that performs massive, fine-grained data reductions. A programmable memory access engine independently fetches and stores data to and from external memory. All three of these components follow their own static schedule provided by the controller compiler. During runtime, the accelerator receives current state measurements and any task-specific information from external sensors. The *RoboX* accelerator carries out the statically schedule generated according to the programmer's high-level specification and solves the corresponding optimization problem. After convergence, the first control input is executed, and the process repeats for the next time step. We discuss the details of the *RoboX* programming interface in the next section.

IV. DSL FOR ROBOTIC CONTROL

RoboX constructs a novel domain-specific language (DSL) to meet the following criterion: (1) provide a **modular** interface which distills optimal control into its core components and (2) be close to the **concise** mathematical expressions while remaining **independent** of implementation. We decompose MPC problems into model and objective formulation. The *RoboX* language provides `System` and `Task` components to represent these elements in a modular fashion. We tackle the second criteria through symbolic computation and group operations. This approach circumvents the need for explicit loops, allowing the code implementation to be independent and simplifying parallelism identification. By keeping

Table I: Language constructs of *RoboX*.

Type	Keyword	Description
Component	System	Definition of robot type comprising all necessary attributes
	Task	Task definition comprising penalties and constraints
Data Types	input	Robot control input
	state	Robot system state
	param	Constant parameter
	penalty	Term minimized during Task execution
	constraint	Constraint on terms in Task
	reference	Potentially time-varying term used to define penalties
	range	Defines an range for array access and group operations
Fields	lower_bound, upper_bound	Inequality constraints on a variable
	equals	Equality constraints on a variable
	running	Indicates enforced everywhere except last step of horizon
	terminal	Indicates enforced only at last step of horizon
	dt	Time derivative of state variable
	weight	Relative weight of penalty term
Mathematical Operations	+,-,*,/	Elementary operators
	sin, cos, ..., sqrt	Nonlinear operations
	sum, norm, min, max	Group operations

the abstraction at the level of constrained optimization, we avoid tying the program to implementation-specific decisions, such as choice of solver or discretization method.

A. System Components

A system definition is denoted using the **System** construct and encapsulates all states, control inputs, constraints, and robot dynamics. The **state** and **input** keywords declare the robot states and control inputs, respectively. Both are composite datatypes that consist of **lower_bound** and **upper_bound** fields, which express physical constraints of the robot. Additionally, the **state** datatype contains a **dt** field, which represents the state time derivative. Constant parameters are defined with the **param** keyword. A summary of all the keywords in the *RoboX* language are provided in Table I. We illustrate the **System** definition of a simple mobile robot in the following code snippet.

```
System MobileRobot( param vel_bound ) {
  // system states
  state pos[2], angle;
  // system inputs
  input vel, ang_vel;
  // system dynamics
  pos[0].dt = vel * cos(angle);
  pos[1].dt = vel * sin(angle);
  angle.dt = ang_vel;
  // physical constraints
  vel.lower_bound <= -vel_bound;
  vel.upper_bound <= vel_bound;}
```

The above **System** component defines the robot's **state** using the 2D array `pos` and `angle` variables, which correspond to the robot's position and orientation, respectively. The control inputs are the velocity (`vel`) and the angular velocity (`ang_vel`). *RoboX* offers two forms of assignments, symbolic (=) and imperative (<=). Imperative expressions are immediately evaluated in program order and are used for expressing physical constraints and parameters. For example, the **lower_bound** and **upper_bound** fields of the control input `vel` above are imperatively assigned. Symbolic expressions declare the formal relationship between variables, such how the state derivative relates to the other states and the control inputs. In the snippet above, the time derivatives of the position states are symbolically assigned to each element of the vector's **dt** field. These symbolic variables can be used in other symbolic expressions to compose more complex mathematical functions.

B. Task Components

The second component of a *RoboX* program is a description of the robot's task. A task is broken down into a series of penalty terms and task-specific constraints. The construct **Task** denotes

a task definition, and the **penalty** and **constraint** keywords are used to specify the penalty terms and constraints, respectively. Both are assigned expressions which contain at least one **state** or **input** variable. A **penalty** has a **weight** field, which sets the relative penalty weight in the objective (default is one). The **constraint** variable has **lower_bound** and **upper_bound** fields to express inequality constraints and an **equals** field to define an equality constraint. Going back to the mobile robot, we provide an example which instructs the robot to move to a fixed target.

```
System MobileRobot(...) {
  Task moveTo(
    reference desired_x,
    reference desired_y,
    param weight,
    param radius) {
    // penalize distance from target
    penalty target_x, target_y;
    target_x.terminal = pos[0] - desired_x;
    target_y.terminal = pos[1] - desired_y;
    target_x.weight <= weight;
    target_y.weight <= weight;
    // constraints on position
    constraint pos_bound;
    pos_bound.running = pos[0]^2 + pos[1]^2;
    pos_bound.upper_bound <= radius;} }
```

The code snippet defines a task `moveTo`, which specifies terminal penalties, `target_x` and `target_y`. The penalty is the difference between some fixed constant location (`desired_x`, `desired_y`) and the robot's current location (`pos[0]`, `pos[1]`). This encourages the robot towards the target location at the end of the trajectory. A running constraint term `pos_bound` is defined which instructs the robot to be within a circle of radius `radius`. The penalties and constraints are indicated as running or terminal by assigning the expression the variable's **running** or **terminal** field, respectively. The example also introduces the **reference** datatype, which is used to express information from external sources. For example, the target location `moveTo` may be determined by an external device performing object detection. We illustrate how to utilize references through the following example.

```
reference desired_x;
reference desired_y;
MobileRobot robot(0.1, 0.01);
robot.moveTo(desired_x, desired_y, 1);
```

A `MobileRobot` is instantiated as `robot` and the desired task is called like a method. The references `desired_x` and `desired_y` are defined globally and passed to the `moveTo` task.

C. Mathematical Operations

The *RoboX* DSL also supports a wide range of mathematical operations. Although our DSL's mathematical expressions share a resemblance to the language in TABLA [19], the latter offers neither symbolic constructs nor complex primitives that enable expressing the robot physics. Supported operations are categorized into (1) elementary, (2) nonlinear, and (3) group operations, as shown in Table I. Elementary operations consist of addition (+), subtraction (−), multiplication (∗), and division (/). Nonlinear operations comprise nonlinear functions such as `cos`, `sin`, `tan`, `acos`, `asin`, `atan`, `exp`, and `sqrt`. Both types may be used to compose symbolic or imperative expressions. The *RoboX* language performs operations over multi-dimensional variables with group operations. Group operations are declared with the **range** datatype, which provides a concise means to express accesses over multi-dimensional variables
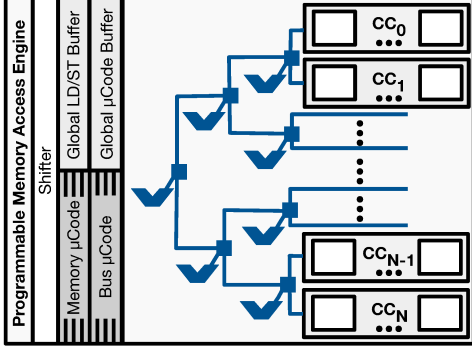
Figure 3: *RoboX* architecture which comprises: a hierarchical composition of Compute Units (CUs) into Compute Clusters (CCs); a compute-enabled interconnect; and a memory access engine.

without the need for explicit loops. Supported group operations include `sum`, `norm`, `min`, and `max`. A `sum` operation adds the elements of an expression over the range indicated by the **`range`** variable and yields a scalar. Similarly, a `norm` computes the Euclidean norm and `min` and `max` operations compute the min and max of an expression. For instance, the constraint `pos_bound` in the `moveTo` task is actually a norm operation over the position vector:

```
range i[0:2];
pos_bound[i].running = norm[i](pos[i]);
```

In this example, the **`range`** variable `i` is defined over the interval $[0, 2)$. We can also use a **`range`** variable coupled with group operations to perform matrix operators:

```
state x[2], R[2][2];
range i[0:2], j[0:2];
x[i].dt = sum[j](R[i][j] * x[j]);
```

In this example, the time derivative of the state vector x corresponds to $\partial x_i / \partial t = \sum_j R_{ij} \times x_j$. The range for the group operation is provided in the brackets while the expression is placed within the parenthesis. The **`range`** variables `i` and `j` correspond to the indices in the mathematical formulas that implicitly define a loop. These variables help *RoboX* identify sources of parallelism in the computations. For instance, it is clear from the code snippet that the computation of each element `x[i].dt` is independent.

RoboX's DSL aims to provide constructs that enable expressing mathematical formulas in a textual representation with an almost one-to-one correspondence. From this DSL, *RoboX* automatically maps the robot dynamics and solver computation to the accelerator after inserting the parameterized solver code. The next section discusses the unique architecture of *RoboX*'s programmable accelerator and how it provides the necessary flexibility for the robotics domain.

V. ACCELERATOR ARCHITECTURE

In devising the *RoboX* architecture, we aim to exploit parallelism available from both the dynamics and solver computations. Data dependencies between operations during dynamics computation for a given time step have limited instruction-level parallelism. In contrast, much of the solver computation involves matrix operations, which exhibit more data parallelism. Therefore, we chose a flexible dataflow architecture to support these two distinct workload phases. As Figure 3 illustrates, the accelerator architecture is organized into a two-level hierarchy of Compute Clusters (CCs), each of which contain a set of Compute Units (CUs). High data dependency dataflow graphs necessitate a significant amount of data transfer
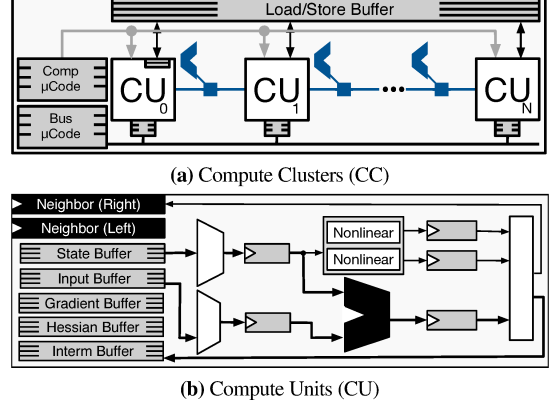

(a) Compute Clusters (CC)

(b) Compute Units (CU)

Figure 4: (a) Single CC composed of multiple CUs, compute-enabled interconnect between neighboring CUs, and shared bus. (b) Single pipelined CU carrying out an arithmetic operation on state and input data and writing to the interim buffer.

from the source units to their destinations. This provides an opportunity to perform some computation in the interconnect rather than the destination. Thus, we propose a compute-enabled interconnection fabric which offers simple compute capabilities over in-flight data.

Additionally, a programmable memory access engine actively fetches data rather than passively responding to requests from compute elements. The interconnect and access engine are programmable to simplify the hardware and avoid complex hardware-based arbitration and handshaking between compute and memory elements. These three elements process their own separate statically-scheduled micro-instructions, detailed in Section VI. The following elaborates on each microprogrammable component.

Compute-enabled interconnect. Enabling computation in the interconnect needs to add minimal overhead to its normal operation. As such, we propose to augment each hop of the busing system with a limited capability functional unit to operate on the in-transit data. In *RoboX*, we add a multiply-add unit, which is frequently used in reduction operations for our target domain. Either the flit of data can specify to perform an operation or a preloaded queue in the hop may contain the schedule for operating on the transiting data. A shift register is sufficient for the hops in the *RoboX*'s architecture, in which the interconnect is preprogrammed with a static schedule and the hops support a single function. A `0` in the shift register indicates that the operation will be bypassed and the normal data delivery is needed. A `1`, on the other hand, engages the functional unit in the hop. As Figure 3 illustrates, the CCs are connected through such a compute enhanced tree-bus interconnect. The tree-bus organization of the CCs is beneficial for reduction patterns, which exhibit high data dependencies and are common in matrix multiplications, Euclidean norms, and other solver operations. To further speed these reduction operations, as depicted in Figure 3, the tree bus employs our compute-enabled interconnect concept as defined above. Note that the complex operations are always deferred to the CUs for execution to avoid over complicating the interconnect.

Within the CC, as Figure 4a shows, the CUs are connected via shared bus and also single-hop connections between neighboring CUs. These single-hop connections facilitate low-overhead communication between neighboring CUs, circumventing the shared bus. These hops also have access a multiply-add unit

to perform operations while passing the data along. While the inter-CU hops can perform aggregation for smaller data arrays, rows of larger arrays can be parallelized across the CCs. Thus, the partial row computation can be performed in a CC and aggregated across the CCs through their compute-enabled interconnect. This feature in the architecture is very useful for parallelizing group operations in the dynamics and penalty computation phases.

Compute clusters. Figure 4a shows a single CC. Each CC contains separate queues for the compute and communication microprograms. These microprogram is the result of statically scheduling the compute and communication instructions. As such, CUs do not initiate communication requests but merely consume data available, simplifying the CC design and busing logic. Communication micro-instructions dictate the inter-CU communication through the shared bus by indicating the source and the destination CU (s). As shown, the CUs are connected to the bus through a FIFO. Shared bus communication follows either a one-to-one, one-to-many, or one-to-all broadcast pattern. This is of particular importance in dynamics computation, where multiple CUs may require the same piece of data produced by a single CU in the CC. The compute micro-instructions determine the operations for all CUs in the CC. The CUs can perform distinct operations on unique data to exploit the fine-grained parallelism in the DFG, or the CC can operate in SIMD mode through vector operations. The SIMD mode is useful for performing element-wise multiplication on arrays, while the inter-CU compute-enabled hops aid in reduction of the products. Both SIMD mode and compute-enabled interconnect assists in efficiently performing group operations in the robot dynamics and task penalty computation.

Compute unit. Figure 4b illustrates the organization of a single CU, which comprises buffers, registers, ALU, nonlinear operations look up tables, and associated busing logic. We separate the CU memory into separate buffers according to a set of namespaces allocated by the ISA, as discussed in Section VI. Demarcating the buffers allows for parallel access to provide all operands simultaneously. Buffers are implemented as queues, where each element can be optionally popped and discarded or rewritten back to enable reuse. Dedicated registers enable communication between neighboring CUs. Each CU has a three-staged pipeline that access, compute, and write the data. Supported operations are addition, subtraction, multiply, and nonlinear functions as lookup tables. Due to large area of division, it is only supported by one CU per CC. Similarly, to prevent the excessive overhead of large LUTs for every nonlinear operation, each CU only supports two such operations.

Programmable memory access engine *RoboX* provides a memory access engine, programmed according to the static schedule of the operations. The programmability allows dealing with misaligned data to prevent bandwidth under-utilization. An integrated *shifter* properly aligns data according to the microprogram loaded into the engine. To hide the latency of external memory accesses, the engine *prefetches* instructions and data according to its schedule and loads them into global instruction and load buffers, respectively. Similarly, all the final results from the compute elements are stored by the access engine based on its microprogram.

Through a compute-enabled interconnect and static microprogramming of the memory access engine, the *RoboX* architecture

allows interconnection and memory to behave as active elements. This design contrasts with traditional architectures, where compute elements actively initiate requests and memory and interconnection subsystems are passive. Next, we discuss *RoboX*'s unique instruction set abstraction to efficiently express the component interactions.

VI. INSTRUCTION SET ARCHITECTURE

To support the *RoboX* architecture, we propose a novel ISA which (1) splits a program into separate compute, communication, and memory instructions; (2) abstracts away hardware implementation details; and (3) allows static scheduling at compile time. Table II shows the instructions in the ISA for each of the three categories, which are all encoded in 32 bits. These high-level instructions are converted to microprograms that represents the schedule for the for the inter- and intra-CC bus, bypass bit patterns, the compute-enabled hops in the interconnect, and operations for the CUs. Additionally, the ISA remains independent of the implementation of the compute-enabled interconnects. Instructions simply express the group operation performed and at what granularity. Below, we discuss the organization of the ISA and the details of the individual instructions.

Namespaces. To simplify the layout of data in memory and facilitate inter- and intra-CC communication, the ISA exposes a set of namespaces which organize data into their respective categories. All instructions share the namespaces INPUT, STATE, GRADIENT, and HESSIAN. Computation and communication instructions also have the namespaces INTERN, LEFT NEIGHBOR, and RIGHT NEIGHBOR. Memory instructions have namespaces REFERENCE and INSTRUCTION. These namespaces semantically separate data and simplify the communication instructions. As discussed in Section V, *RoboX* implements most of these namespaces as queues and registers. The memory namespace INSTRUCTION holds all instructions for *RoboX* to execute. There also needs to be a designated location in memory for external environmental data not captured directly by the state, such as the location of a target or bounds of a racing track. As such, we provide the REFERENCE namespace to hold all such external data relevant for penalty or constraint computation. Memory is partitioned according to these namespaces and determines the layout of all data accordingly.

Compute instructions. The compute instructions dictate the computation local to a given Compute Cluster. The supported functions are the same as the elementary and nonlinear operations provided to the programmer by the *RoboX* language. As Table II shows, these instructions are divided into scalar and SIMD operations and further broken down into queue vs. immediate operations. Scalar instructions indicate the operation to be performed by an individual CU, while SIMD instructions have all the CUs in the CC perform the same operation. Additionally, SIMD instructions use a repeat field, which tells the CC to repeat the SIMD operation a pre-specified number of times but on different data. This strategy reduces the instruction count. Queue instructions require a queue namespace and index to be specified for each source, while immediate instructions allow for one of the sources to be an 8-bit integer. Only the top 8 elements of the queue are addressable. However, each queue-type instruction has a dedicated Pop field which dictates whether the data should remain in the queue after access, discarded after use, or popped and rewritten for later reuse. All of the sources and destinations specified by the instructions are local to the CU which

Table II: The *RoboX* ISA, which is divided into separate compute, communication, and memory instructions.

Bits	31 - 29	28 - 27	26 - 25	24 - 22	21 - 19	18 - 17	16 - 14	13 - 11	10 - 8	7 - 5	4 - 3	2 - 0
Compute												
Scalar Queue Op	Opcode = 000	Function		Destination Namespace	Source 1 Namespace	Source 1 Pop	Source 1 Index	0		Source 2 Namespace	Source 2 Pop	Source 2 Index
Vector Queue Op	Opcode = 001	Function		Destination Namespace	Source 1 Namespace	Source 1 Pop	Source 1 Index	Vector Length		Source 2 Namespace	Source 2 Pop	Source 2 Index
Scalar Imm Op	Opcode = 010	Function		Destination Namespace	Source 1 Namespace	Source 1 Pop	Source 1 Index	0	Immediate			
Vector Imm Op	Opcode = 011	Function		Destination Namespace	Source 1 Namespace	Source 1 Pop	Source 1 Index	Vector Length	Immediate			
Communication												
Unicast	Opcode = 000	Destination PU Quarter	Destination PE Quarter	Destination Namespace	Source Namespace	Source Pop	Source Index	Destination PE	Destination PU	0	Source PE Quarter	Source PE ID
PE Multicast	Opcode = 010	Destination PE Quarter Mask		Destination Namespace	Source Namespace	Source Pop	Source Index	PE Mask			Source PE Quarter	Source PE ID
PU Multicast	Opcode = 011	Destination PU Quarter Mask		Destination Namespace	Source Namespace	Source Pop	Source Index	PU Mask			Source PE Quarter	Source PE ID
Broadcast	Opcode = 111	0		Destination Namespace	Source Namespace	Source Pop	Source Index	0			Source PE Quarter	Source PE ID
PE Aggregation	Opcode = 100	Destination PE Quarter Mask		Destination Namespace	Source Namespace	Source Pop	Source Index	PE Mask			Function	0
PU Aggregation	Opcode = 101	Destination PU Quarter Mask		Destination Namespace	Source Namespace	Source Pop	Source Index	PU Mask			Function	0
Memory												
Load	Opcode = 000	Offset				Shift Amt	PE Mask				PE Quarter	Namespace
Store	Opcode = 001	Offset				Shift Amt	PE Mask				PE Quarter	Namespace
Set Block	Opcode = 010	Block Number									0	Namespace
End of Code	Opcode = 011	Not Used										

executes it. As such, the CUs are not concerned with data transfer and simply perform computation on data available in the queues.

Communication instructions. Communication instructions shown in Table II orchestrate the intra- and inter-cluster data transfer and in-bus computation. To improve the scalability of the *RoboX* ISA, CUs within a CC and CCs themselves are organized into quarters. Data transfer instructions comprise Unicast, Multicast, and Broadcast communication styles. A Unicast transfers data from a single CU to another, potentially in differing CCs. The multicast type is a one-to-many communication style, where a CU sends data to either a subset of the CUs within its CC (CU Multicast) or to all CUs within a subset of CCs (CC Multicast). A dedicated field indicates the target CU or CC quarter, and mask bits are used to specify the recipient CU or CC within the quarter. Finally, the Broadcast instruction transfers a data element from a single CU to *all* the CUs on the accelerator.

Compute-enabled interconnect instructions. Instructions for the compute-enabled interconnect include CU Aggregation and CC Aggregation, which perform a pre-specified group operation over the CUs within a CC or across all CCs, respectively. The supported aggregation functions are ADD, MUL, MIN, and MAX. Group operations in the DSL are compiled to a combination of in-bus aggregation and SIMD operations. The sum, min, and max group operations can be implemented directly with their corresponding aggregation functions. However, the norm function can not be implemented with a single aggregation instruction. Instead, this operation is carried out by sequentially applying a MUL aggregation, an ADD aggregation, and a SQRT operation on the result.

Memory instructions. As discussed above, the memory is also organized into different namespaces. Each portion of memory corresponding to a namespace is further subdivided into multiple blocks to enable a fixed-sized instruction to access the full range of memory addresses. The namespace and offset from the current namespace's block pointer is provided as a field in the Load and Store instructions. A Set Block instruction changes the current block number to the one specified for the indicated namespace. Furthermore, as the ISA is designed to be statically scheduled, *RoboX* leverages this blocking to organize data in the memory efficiently. To cope with data misalignments, the Load and Store instructions also provide a shift field.

VII. COMPILATION WORKFLOW

The compilation workflow has two phases: (1) *Program Translator* and (2) *Controller Compiler*. The Program Translator takes as input a *RoboX* program and generates a M-DFG of the entire MPC algorithm. The Controller Compiler uses this M-DFG to generate the final static schedules.

Program Translator. In *RoboX*, the solver and discretization method are fixed, allowing us to express it as an invariant yet parameterized code. These parameters are set by the dynamics, penalties, and constraints defined by the *RoboX* program, as well as the meta-parameters, such as the horizon length and desired controller rate. The Program Translator first assigns an ordering to the states and inputs of the robot. It organizes penalties and constraints into separate running and terminal groupings. The objective function is a summation of the weighted Euclidean norms of each penalty $\sum_i ||p_i||^2_{W_i}$, where W_i is a diagonal matrix of each weight assigned to the penalty's **weight** field. The Program Translator extracts the computation for each of these components and uses automatic differentiation to compute all necessary gradients. Each construct in the *RoboX* language has a corresponding M-DFG node representation. Elementary and nonlinear operations are simply single SCALAR type nodes with edges expressing its dependencies. Any elementary or nonlinear operation which is defined over an interval specified by a **range** variable is a VECTOR node. Lastly, group operations are represented by single GROUP aggregation node. Internally, a GROUP node is a ARRAY node which also specifies the aggregation to perform over its results. The Program Translator constructs the final M-DFG by generating the nodes of all the expressions in the *RoboX* program and merging them according to its solver template.

Controller Compiler. The Controller Compiler takes the M-DFG as input and constructs separate operation, data, communication, and aggregation maps. Specifically, the operation map assigns all the M-DFG operations to the CUs except for those executed in the interconnection fabric. The aggregation map keeps track of the CUs which provide results to be aggregated for a given group operation. The data map determines the assignment of states, inputs, penalties and all associated KKT, constraints, and reference variables. Finally, the communication map enumerates which CUs receive each piece of produced data during program execution.

The controller compiler first constructs an initial data map D by pre-assigning the location of DFG operands, or graph edges, which correspond to state or input variables. This data is assigned according to the CU ordering determined by Program Translator, number of prediction time steps, and number of states in the robot model. The Controller Compiler uses an Algorithm 1 to generate mappings and takes as input the DFG graph, initial data map D, number of CUs per CC (n_{cu}), and the total number of CUs (n_{total}). Its output is a program map M, which contains an operation ($M.O[n_{total}]$) and data ($M.D[n_{total}]$) map as an array of lists indexed by the CU. There is also a communication ($M.C[|E|]$)

```
Input: M-DFG: Dataflow graph (V, E)
       D: Initial data map
       n_cu: Number of CUs per CCs
       n_total: Total number of CUs
Output: M: Program map
Initialize M ∀ types ← ∅
Initialize G ← M-DFG
Initialize cu_idx = 0
while (G ≠ ∅) do
    if (∃ v ∈ G s.t. p_i = ASSIGNED ∀p_i ∈ v.parents) then
        for (op ∈ v.ops) do
            if (∃ src_i ∈ op.src, cu_i ∈ src_i s.t. cu_i ≠ NULL) then
                if (∃ src_j ∈ op.src s.t. cu_j = NULL ∀ cu_j ∈ src_j) then
                    src_j.append(cu_i)
                    M.D[cu_i].append(src_j)
                else if (∃ src_j ∈ op.src s.t. cu_j ≠ cu_i ∀ cu_j ∈ src_j) then
                    M.C[src_j].append(cu_i)
                M.O[cu_i].append(op)
                if (v.type = GROUP) then
                    M.A[v].append(cu_i)
            else if (cu_i = NULL ∀cu_i ∈ src_i, src_i ∈ op.src) then
                for (src_i ∈ op.src) do
                    src_i.append(cu_idx)
                end
                M.O[cu_idx].append(op)
                if (v.type = GROUP) then
                    M.A[v].append(cu_idx)
                end
                cu_idx = (cu_idx + 1) % n_total
        end
        G.remove(v)
end
```

Algorithm 1: Compute-Enabled Interconnect-Aware Mapping.

map which is indexed by an edge of the DFG and stores the CUs to which that data should be sent. Similarly, there is an aggregation map ($M.A[|V|]$) which is indexed by the vertex of a GROUP operation. The algorithm then proceeds as follows:

1) **Initialize** the operation, communication, and aggregation maps to null, the data map to D, the graph variable G to the *M-DFG*, and zero the CU counter (cu_{idx}).

2) **Select a ready vertex** (v), meaning all its parents have been assigned. Then, iterate through all operations (op) in vertex v. SCALAR nodes will only have one operation.

3) **Check if a source has been mapped** (src_i) for op in vertex v. If not, assign all source nodes to CU counter (cu_{idx}) and proceed to step (5).

4) **Check for second source** (src_j) of op in vertex v. If it exists and is not mapped, assign it to src_i's CU and set the data map accordingly. Otherwise, inform the communication map that src_j should be sent to src_i's CU.

5) **Assign the operation** op to the CU. If v is of type GROUP, add the CU to the aggregation list for vertex v.

6) **Reiterate** steps 2 through 6 until all vertices are mapped.

The Controller Compiler then uses M to statically schedule all operations, communication, and memory accesses. From the location of the CUs in each GROUP vertex aggregation map, the aggregation is either performed over the inter-CU hops in a CC or in the compute-enabled tree-bus.

VIII. EVALUATION

Benchmark Robots and Tasks. Table III lists the six benchmark robot systems used to evaluate *RoboX*, which consist of a variety of types of robotic systems. In particular, MobileRobot [21] is a two-wheeled mobile robot employed in a trajectory tracking task. The Manipulator [24] is an arm-like robot comprising a cascade of joints and links. We consider a two-link manipulator executing a reaching task. The AutoVehicle [20] is a four-wheel autonomous vehicle moving on a racing task, where the goal is to maximize velocity. The racing track bounds correspond to position constraints

Table III: Benchmarks and their model/task parameters.

Name	System	Task	States	Inputs	Penalties	Constraints
MobileRobot	Two-Wheel Mobile Robot	Trajectory Tracking	3	2	5	2
Manipulator	Two-Link Manipulator	Reaching	4	2	6	10
AutoVehicle	Four-Wheel Vehicle	High-Speed Racing	6	2	8	8
MicroSat	Miniature Satellite	Orbit Control	8	4	12	12
Quadrotor	Four-Rotor Micro UAV	Motion Planning	12	4	10	7
Hexacopter	Six-Rotor Micro UAV	Attitude Control	12	6	19	10

Table IV: Specifications of the baselines and *RoboX*.

Platform	Cores	Clock Freq (GHz)	Memory (GB)	TDP (W)	Technology (nm)
ARM Cortex A57	2 + 4	2	2	2.5	16
Intel Xeon E3-1246 v3	4	3.6	16	84	22
Tegra X2	256	0.854	2	7.5	28
GTX 650 Ti	768	0.928	1	110	28
Tesla K40	2880	0.875	12	235	28

RoboX	
# PEs	256
Clock Freq	1 GHz
Memory	512 KB
LUT Entries	4096
Total Power	3.4 W
Technology	45 nm
Peak Bandwidth	128 Gb/s
Area	8.13 um^2

on the car. The MicroSat [22] is a miniature satellite of low mass which must remain in proper orbit under potential disturbances. The Quadrotor [23, 27] and Hexacopter [6] are four- and six-rotor micro UAVs, respectively. Both are engaged in motion planning and orientation control, but have differing dynamics and constraints. This, in turn, changes the computational requirements of the controller. Table III lists each robot, which has differing numbers of states, inputs, and physical constraints and an associated task with a certain number of penalty terms and task-specific constraints. However, the computational requirements of each benchmark do not only depend on these parameters. For each time step in the horizon, the system dynamics, task penalty terms, and constraints need to be evaluated. The complexity of dynamics may significantly vary between robotic systems, even with a similar number of states and/or inputs. For instance, while Quadrotor and Hexacopter have the same number of states, the dynamics of the latter is more computationally intensive. The same is true for the computational requirements for different penalty terms and constraints between tasks.

A. Methodology

CPU Platforms As shown in Table IV, we compare *RoboX* to two multicore CPUs running Ubuntu Linux version 16.04: (1) a high performance quad-core Intel Xeon E3 and (2) a low-power quad-core ARM Cortex A57 available on the Nvidia Jetson TX2. The baseline CPU implementation uses the ACADO Toolkit [34] to implement the optimized, self-contained C code. The code is compiled with GCC 5.4 with *-O3 -ftree-vectorize* to enable aggressive compiler optimization and vector operations for all platforms. The benchmarks use four threads on ARM and eight on Xeon, which supports simultaneous multithreading. ACADO is a high-level framework which supports multiple solvers. We chose the sparsity-exploiting HPMPC interior-point solver, as it demonstrated superior runtime performance over the other options. For a fair comparison, we use the same solver algorithm in *RoboX*. The HPMPC solver uses BLASFEO [38], which is a BLAS-like library tailored for small to medium matrices (up to a few hundred elements). For larger horizons, we used BLASFEO as a wrapper for the standard BLAS implementations.

GPU Platforms We also compare *RoboX* with the three GPUs shown in Table IV: (1) a low-power Tegra X2 available on the Nvidia Jetson TX2, (2) a desktop-class GeForce GTX 650 Ti, and
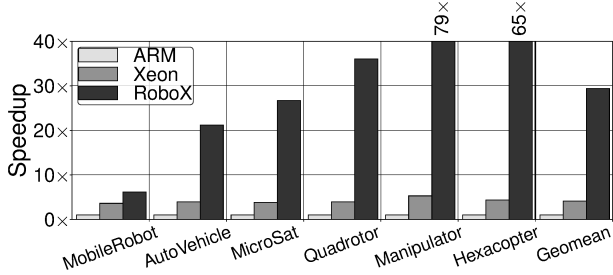
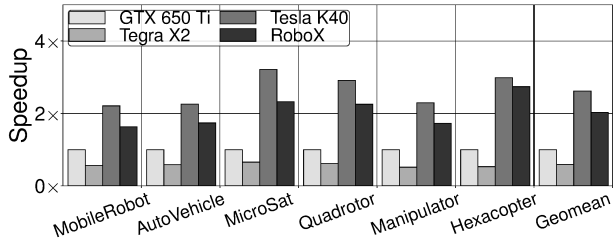Figure 5: Speedup of Xeon E3 and *RoboX* over ARM A57 baseline.

Figure 6: Speedup of GPUs and *RoboX* over GTX 650 Ti baseline.

(3) a high-performance Tesla K40. Due to limited GPU implementations of interior-point solvers, we compared *RoboX* with our custom GPU code written in CUDA using cuBLAS. We made our best efforts to hand-tune the code for each GPU platform and optimize the number of blocks and threads-per-block. All benchmarks were compiled separately for each GPU using target-specific flags.

Execution time measurements. To obtain the execution time measurements for the CPUs and GPUs, we calculate the average based off the measured wall clock time of 10000 solver iterations. For the *RoboX* runtime estimates, we use a custom cycle-accurate simulator with parameters in Table IV. From our empirical study, we found 32-bit fixed-point with 17 fractional bits and 4096-entry LUTs were sufficient to make the effects on convergence negligible.

Power measurements. For the Xeon E3, we use the Intel Running Average Power Limit (RAPL) energy consumption counters available in the Linux Kernel. As the GTX 650 Ti does not support the NVML library but has the same microarchitecture as the Tesla K40, we make a conservative estimation of its power consumption by scaling the Tesla K40 measurements using the ratio of their TDPs. The ARM A57 and Tegra X2 are part of the Jetson TX2 development board, which does not provide a software mechanism to measure energy. Instead, we use the Keysight E3649 Programmable DC Power Supply to measure the power consumption. We subtract the idle average power consumption from the benchmark execution power reading. For the *RoboX* ASIC, we synthesized the accelerator with the Synopsys Design Compiler (L-2016.03-SP5) using TSMC's 45-nm high Vt standard cell libraries to generate area and power estimates. As shown in Table IV, the synthesized accelerator has 512 KB of on-chip memory, an area of 8.13 um^2, consumes 3.4 W, and operates at 1.0 GHz.

B. Experimental Results

CPU performance comparison. Figure 5 shows the speedup of *RoboX* and the Xeon E3 over an ARM A57 baseline for a prediction horizon of 32 steps. On average, *RoboX* has a 29.4× (7.3×) speedup over the ARM A57 (Xeon E3). The performance improvement ranges between 6.2× to 79.1× across the benchmarks. This variation can be attributed to the differences
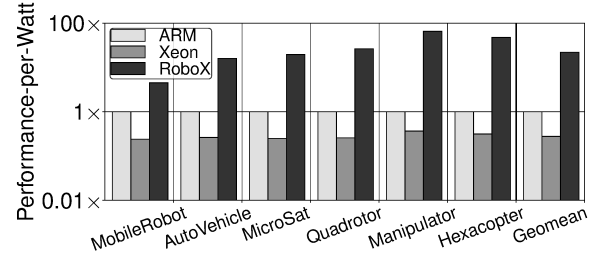

Figure 7: Performance-per-Watt improvement of Xeon E3 and *RoboX* over ARM A57 baseline.
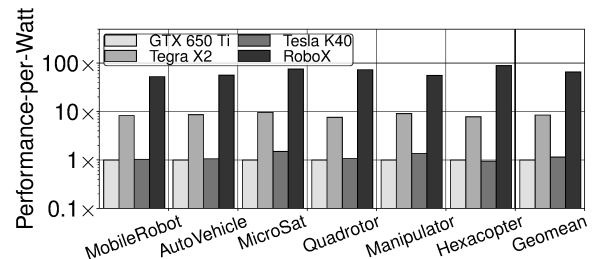

Figure 8: Performance-per-Watt improvement of GPUs and *RoboX* over GTX 650 Ti baseline.

in the robot configurations and computational demands of different dynamics and tasks. For instance, `MobileRobot` has the lowest speedup, as it has least number of states, penalties, and constraints. In several cases, the observed speedup with *RoboX* is proportional to the number of states and complexity of the dynamics. The `Hexacopter` benchmark has the second largest speedup and has the greatest number of penalty terms and control inputs. In some other cases, such as the `Manipulator` benchmark, the complexity of the dynamics exposes enough opportunity for the accelerator to provide greater benefits despite a lower number of states.

GPU performance comparison. Figure 6 illustrates the speedup of *RoboX* compared with the Tegra X2 and Tesla K40 with a GTX 650 Ti baseline. *RoboX* provides an average speedup of 2.0× (3.5×) over the GTX 650 Ti (Tegra X2) for a prediction horizon of 32 steps. These benefits vary between 1.63× (2.89×) and 2.74× (5.17×) over the GTX 650 Ti (Tegra X2). In contrast, *RoboX* is 1.3× slower than the Tesla K40 on average. This is due to the fact that the Tesla has over twice the number of cores and operates under significantly greater power budget of 235 W.

Performance-per-Watt comparison. The computational resources for autonomous robotics often have to function under a tight power budget. Thus, to evaluate the performance benefits for a fixed energy consumption, we use the performance-per-watt as a metric of comparison. Figure 7 shows the performance-per-watt improvement of *RoboX* and the Xeon E3 over the ARM A57 baseline. *RoboX* achieves an average improvement of 22.1× over the ARM A57 baseline, with a range of 4.5× to 65.3×. As expected, the Xeon E3 has a 0.28× lower performance-per-watt over the ARM A57 on average. Over the GPU baselines, *RoboX* achieves an average improvement of 65.5× over the GTX 650 Ti, with a range of 52.5 to 88.4×. The performance-per-watt improvement over the Tegra X2 is 7.8×, as the Tegra functions under a tighter power budget of 7.5 W. In comparison to the Tesla, *RoboX* has an average performance-per-watt improvement of 71.8×.Thus, despite the higher performance benefits of the Tesla, *RoboX* delivers much
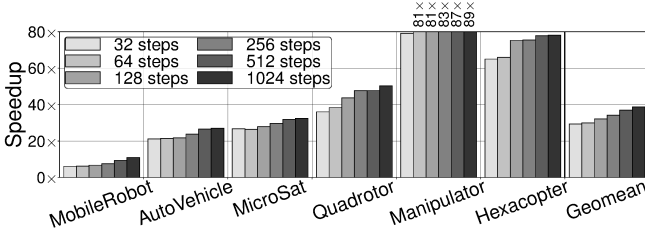
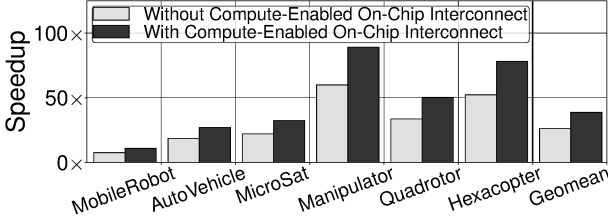Figure 9: Speedup of *RoboX* over ARM A57 baseline for different numbers of prediction horizon time steps.

Figure 10: Average speedup of *RoboX* with and without the compute-enabled on-chip interconnect over ARM A57.
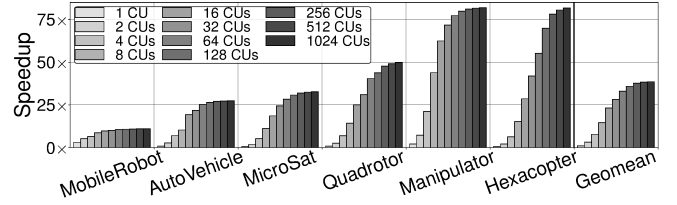

Figure 11: Sensitivity of *RoboX* speedup over ARM A57 to number of Compute Units (CUs).

Figure 12: Sensitivity of *RoboX* speedup over ARM A57 to off-chip memory bandwidth.

higher efficiency under a limited power budget.

To summarize, these results suggest that *RoboX* delivers a higher performance than Xeon, GTX 650 Ti, and the Tegra X2 with an improved power efficiency, even better than the ARM. These improvements demonstrate the suitability of *RoboX* for high-performance under a tight power budget, which is attractive for a variety of robotics applications.

Prediction horizon sweep. Controller performance often improves with longer prediction horizons, but increases the amount of computation performed at each controller invocation. Figure 9 shows the speedup of *RoboX* over different prediction horizon lengths. On average, the speedup grows proportionally with the horizon length, from $29.4\times$ to $38.7\times$. However, different benchmarks are more sensitive to larger horizons than others. For instance, the `Hexacopter` benchmark has the greatest change in speedup for larger horizons, as it has the greatest number of penalty terms. It is also tied for greatest number of states with the `Quadrotor`, but the `Hexacopter` has more average computation per state. Thus, there are more opportunities for parallelism compared to smaller models.

Compute-enabled on-chip interconnect. To illustrate the benefits of the compute-enabled on-chip interconnect, Figure 10 shows the speedup of *RoboX* with and without the interconnect ALUs for a horizon length of 1024 steps. On average, *RoboX* without the interconnect ALUs achieves an average speedup of $25.2\times$, compared with the $38.7\times$ average speedup gained with the compute-enabled interconnect. Overall, the compute-enabled on-chip interconnect provides $\sim 35\%$ increase in average performance.

C. Design Space Exploration

Number of compute units. While the number of CUs for *RoboX* is fixed, we performed a design space exploration by varying the number of CUs across each benchmark. Figure 11 shows the speedup sensitivity to the amount of computational resources available with the ARM A57 baseline. As the amount of parallelism in the application is dependent on the prediction horizon, we explore the case where the prediction horizon is 1024 steps. Except for the `MobileRobot` benchmark, which has the least amount of computation, the speedup initially grows linearly with the number of CUs. Note that we double the number computational resources, starting

from 1 CU to 1024 CUs. However, the benefits generally plateau around 256 CUs, as the maximum amount of parallelism in the solver computation is approached. After 256 CUs, there are diminishing returns due to the minimal change in performance and an increase in power consumption due to the presence of more resources.

Bandwidth sensitivity. Planning and control tasks are both compute and data intensive, as new state and environmental information, as well as the previous solution, are fetched every controller invocation. Thus, the amount of data retrieved from memory grows with the prediction horizon. While the bandwidth of *RoboX* is fixed, we perform a sensitivity study to evaluate the effects of bandwidth on the speedup. Figure 12 shows the speedup of *RoboX* over the ARM A57 baseline for a prediction horizon of 1024 across different bandwidth design points. Intuitively, larger robot models are most sensitive to the increase in bandwidth due to the increase in data. This is particularly true for the `Hexacopter` benchmark, where its speedup varies from $46.1\times$ to $94.3\times$. While all of the models benefit from increased bandwidth, there are diminishing returns up to a certain point due to This is due to the execution time becoming increasingly dominated by computation.

IX. RELATED WORK

Programmable acceleration. Programmable accelerators have received much attention due to their potential for large gains in efficiency and performance by restricting the workload. Traditional approaches to acceleration rely on identifying and mapping compute intensive kernels to specialized hardware [39]–[48]. Recent work has increasingly focused on developing accelerators for a limited set of applications, particularly machine learning and deep neural networks [11]–[19]. While these previous works have shown significant benefits for a subset of learning applications, they are not directly extensible to robot motion planning and control workloads. In *RoboX*, we delve into the theory of motion planning and control for robots to leverage commonalities and provide an end-to-end acceleration solution which can target a wide range of robotic applications.

Hardware implementations for MPC. There have been several efforts to provide hardware support for MPC algorithms. Prior ASIC designs [49, 50] for MPC do not offer the flexibility to support different robotic models and are also limited to linear

10

dynamics. Furthermore, existing FPGA implementations [51]–[57] are also problem-specific, as they restrict the MPC to first-order gradient solvers or even a specific system-task pairs. Recent work uses HLS to accelerate nonlinear MPC with FPGAs [58]–[62]. In contrast, *RoboX* is not focused on one or a set of robotics applications and does not restrict the dynamics of the robot. *RoboX*, on the other hand, provides a comprehensive programable ASIC acceleration including a novel DSL and architecture with features like the compute-enabled interconnect.

Domain-specific languages for robotics. Existing DSLs for expressing robot kinematics and dynamics are designed to compose simple, pre-specified primitives together [63]–[66]. However, these languages often limit themselves to specific robot types, such as multi-link manipulators, and do not provide any task-specific information to generate an actual controller. Languages which focus on task specification generate simpler control algorithms and do not support MPC or rely on pre-specific action primitives for particular types of robots [67]–[76]. Other approaches, such as ACADO [31]–[34], expose a high-level API to generate optimized C code. Instead, *RoboX* provides a mathematical DSL backed by a compiler and hardware architecture. This DSL does not limit the programmer to pre-specified elements and allows the expression of a wide variety of applications.

Software parallelization for MPC. Alternative approaches leverage algorithmic approximation techniques to enhance the parallelism of MPC [77, 78]. These purely software-based implementations deliver faster performance at the cost of control accuracy and robustness. *RoboX* is orthogonal to these approximation techniques and can incorporate them to provide additional benefits.

In-network computation. As an emerging area, recent works have explored delegating parts of execution to Network Interface Cards (NICs), routers, and switches [79]–[83]. In contrast, this paper defines the on-chip compute-enabled interconnects.

X. Conclusion

Robotics and automation have been continuously transforming a wide range of industries. As advances continue in robotics, their computational demand is increasing. As such, this work sets out to accelerate autonomous robotics by providing the cross-stack solution of *RoboX*. This solution abstracts away the complicated details of control theory, optimization formulation, hardware, and its micro-programming from developers, yet delivers significant performance and efficiency gains. While efficiency is crucial, wide range of applicability is vital for adoption of accelerators. As such, *RoboX* utilizes model predictive control to move away from traditional practices of offloading code to specialized hardware and provides an end-to-end acceleration solution that builds upon the theory of robotic control.

References

[1] Curiosity rover. https://mars.nasa.gov/msl/.
[2] The da vinci surgical system. http://www.intuitivesurgical.com/products/davinci_surgical_system/.
[3] Oshbot. http://www.lowesinnovationlabs.com/.
[4] L. Pericca, P. Ohlckers, and C. Grinde, "Micro- and nano-air vehicles: State of the art," in *International Journal of Aerospace Engineering*, 2011.
[5] Phantom 2. https://www.dji.com/phantom-2/.
[6] M. A. M. Kamel, K. Alexis and R. Siegwart, "Fast nonlinear model predictive control for multicopter attitude tracking on so(3)," in *IEEE Multi-Conference on Systems and Control*, 2015.
[7] Z. Zhang, A. Suleiman, L. Carlone, V. Sze, and S. Karaman, "Visual-inertial odometry on chip: An algorithm-and-hardware co-design approach," in *Robotics: Science and Systems (RSS)*, 2017.
[8] M. Keennon, K. Klingebiel, H. Won, and A. Andriukov, "Development of the nano hummingbird: A tailless flapping wing micro air vehicle," in *AIAA Aerospace Sciences Meeting and Exhibit*, 2012.
[9] R. J. Wood, B. Finio, M. Karpelson, K. Ma, N. O. Perez-Arancibia, P. S. Sreetharan, H. Tanaka, and J. P. Whitney, "Progress on 'pico' air vehicles," in *The International Journal of Robotics Research*, 2012.
[10] R. He and S. Sato, "Design of a single-motor nano aerial vehicle with a gearless torque-canceling mechanism," in *AIAA Aerospace Sciences Meeting and Exhibit*, 2008.
[11] T. Chen, Z. Du, N. Sun, J. Wang, C. Wu, Y. Chen, and O. Temam, "DianNao: A Small-footprint High-throughput Accelerator for Ubiquitous Machine-learning," in *ASPLOS*, 2014.
[12] Z. Du, R. Fasthuber, T. Chen, P. Ienne, L. Li, T. Luo, X. Feng, Y. Chen, and O. Temam, "ShiDianNao: shifting vision processing closer to the sensor," in *ISCA*, 2015.
[13] D. Liu, T. Chen, S. Liu, J. Zhou, S. Zhou, O. Teman, X. Feng, X. Zhou, and Y. Chen, "PuDianNao: A polyvalent machine learning accelerator," in *ASPLOS*, 2015.
[14] B. Reagen, P. Whatmough, R. Adolf, S. Rama, H. Lee, S. K. Lee, J. M. Hernandez-Lobato, G. Y. Wei, and D. Brooks, "Minerva: Enabling Low-Power, Highly-Accurate Deep Neural Network Accelerators," in *ISCA*, 2016.
[15] S. Han, X. Liu, H. Mao, J. Pu, A. Pedram, M. A. Horowitz, and W. J. Dally, "EIE: Efficient Inference Engine on Compressed Deep Neural Network," in *ISCA*, 2016.
[16] Y.-H. Chen, J. Emer, and V. Sze, "Eyeriss: A Spatial Architecture for Energy-Efficient Dataflow for Convolutional Neural Networks," in *ISCA*, 2016.
[17] J. Albericio, P. Judd, T. Hetherington, T. Aamodt, N. E. Jerger, and A. Moshovos, "Cnvlutin: Ineffectual-Neuron-Free Deep Neural Network Computing," in *ISCA*, 2016.
[18] H. Sharma, J. Park, D. Mahajan, E. Amaro, J. K. Kim, C. Shao, A. Mishra, and H. Esmaeilzadeh, "From High-Level Deep Neural Models to FPGAs," in *MICRO*, 2016.
[19] D. Mahajan, J. Park, E. Amaro, H. Sharma, A. Yazdanbakhsh, J. K. Kim, and H. Esmaeilzadeh, "TABLA: A Unified Template-based Framework for Accelerating Statistical Machine Learning," in *HPCA*, 2016.
[20] A. Liniger, A. Domahidi, and M. Morari, "Optimization-based autonomous racing of 1:43 scale rc cars," in *Optimal Control Applications and Methods*, 2014.
[21] F. Kuhne, J. M. G. da Silva Jr, and W. F. Lages, "Mobile robot trajectory tracking using model predictive control," in *Latin American Robotics Symposium*, 2005.
[22] O. Hegrenaes, J. T. Gravdahl, and P. Tondel, "Spacecraft attitude control using explicit model predictive control," in *Automatica*, 2005.
[23] S. Bouabdallah and R. Siegwart, "Full control of a quadrotor," in *IEEE/RSJ International Conference on Intelligent Robots and Systems*, 2007.
[24] R. M. Murray, Z. X. Li, and S. S. Sastry, *A Mathematical Introduction to Robotic Manipulation*. CRC Press, 1994.
[25] M. Neunert, C. de Crousaz, F. Furrer, M. Kamel, F. Farshidian, R. Siegwart, and J. Buchli, "Fast Nonlinear Model Predictive Control for Unified Trajectory Optimization and Tracking," in *ICRA*, 2016.
[26] P. Bouffard, A. Aswani, , and C. Tomlin, "Learning-based model predictive control on a quadrotor: Onboard implementation and experimental results," in *IEEE International Conference on Robotics and Automation*, 2012.
[27] G. N. K. Alexis, C. Papachristos and A. Tzes, "Model predictive quadrotor indoor position control," in *MCCA*, 2011.
[28] E. Todorov and W. Li, "A generalized iterative lqg method for locally optimal feedback control of constrained nonlinear stochastic systems," in *ACC*, 2005.

[29] T. Erez, Y. Tassa, and E. Todorov, "Synthesis and stabilization of complex behaviors through online trajectory optimization," in *International Conference on Intelligent Robots and Systems*, 2012.

[30] S. Boyd and L. Vandenberghe, "Interior-point methods," in *Convex Optimization*, 1st ed. Cambridge University Press, 2008.

[31] M. Vukov, A. Domahidi, H. J. Ferreau, M. Morari, and M. Diehl, "Auto-Generated Algorithms for Nonlinear Model Predictive Control on Long and on Short Horizons," in *CDC*, 2013.

[32] B. Houska, H. J. Ferreau, and M. Diehl, "An Auto-Generated Real-Time Iteration Algorithm for Nonlinear MPC in the Microsecond Range," in *Automatica*, 2011.

[33] M. Diehl, R. Findeisen, and F. Allgower, "A Stabilizing Real-time Implementation of Nonlinear Model Predictive Control," in *Real-Time and Online PDE-Constrained Optimization*, L. Biegler, O. Ghattas, D. K. M. Heinkenschloss, and B. van Bloemen Waanders, Eds. SIAM, 2007.

[34] B. Houska, H. J. Ferreau, and M. Diehl, "ACADO Toolkit - An open-source framework for automatic control and dynamic optimization." in *Optimal Control Applications and Methods*, 2010.

[35] A. Domahidi, A. U. Zgraggen, M. N. Zeilinger, M. Morari, and C. N. Jones, "Efficient Interior Point Methods for Multistage Problems Arising in Receding Horizon Control," in *CDC*, 2012.

[36] J. Mattingley and S. Boyd, "Automatic Code Generation for Real-Time Convex Optimization," in *Convex Optimization in Signal Processing and Communication*, 2009.

[37] L. N. Trefethen and D. B. III, "Cholesky factorization," in *Numerical Linear Algebra*, 1st ed. SIAM, 1997.

[38] G. Frison, D. Kouzoupis, A. Zanelli, and M. Diehl, "BLASFEO: Basic Linear Algebra Subroutines for Embedded Optimization," in *ArXiV*, 2017.

[39] G. Venkatesh, J. Sampson, N. Goulding, S. Garcia, V. Bryksin, J. Lugo-Martinez, S. Swanson, and M. B. Taylor, "Conservation cores: Reducing the energy of mature computations," in *International Conference on Architectural Support for Programming Languages and Operating Systems*, 2010.

[40] H. Esmaeilzadeh, A. Sampson, L. Ceze, and D. Burger, "Neural acceleration for general-purpose approximate programs," in *MICRO*, 2012.

[41] R. S. Amant, A. Yazdanbakhsh, J. Park, B. Thwaites, H. Esmaeilzadeh, A. Hassibi, L. Ceze, and D. Burger, "General-purpose code acceleration with limited-precision analog computation," in *ISCA*, 2014.

[42] A. Yazdanbakhsh, J. Park, H. Sharma, P. Lotfi-Kamran, and H. Esmaeilzadeh, "Neural acceleration for gpu throughput processors," in *MICRO*, 2015.

[43] V. Govindaraju, C.-H. Ho, T. Nowatzki, J. Chhugani, N. Satish, K. Sankaralingam, and C. Kim, "Dyser: Unifying functionality and parallelism specialization for energy-efficient computing," in *MICRO*, 2012.

[44] A. Putnam, D. Bennett, E. Dellinger, J. Mason, P. Sundararajan, and S. Eggers, "Chimps: A c-level compilation flow for hybrid cpu-fpga architectures," in *International Conference on Field Programmable Logic and Applications*, 2008.

[45] N. Clark, M. Kudlur, H. Park, S. Mahlke, and K. Flautner, "Application-specific processing on a general-purpose core via transparent instruction set customization," in *MICRO*, 2004.

[46] Z. A. Ye, A. Moshovos, S. Hauck, and P. Banerjee, "Chimaera: A high-performance architecture with a tightly-coupled reconfigurable functional unit," in *ISCA*, 2000.

[47] J. R. Hauser and J. Wawrzynek, "Garp: A mips processor with a reconfigurable coprocessor," in *IEEE Symposium on FPGA-Based Custom Computing Machines*, 1997.

[48] K. Fan, M. Kudlur, G. Dasika, and S. Mahlke, "Bridging the computation gap between programmable processors and hardwired accelerators," in *HPCA*, 2009.

[49] K. Karagianni, T. Chronopoulos, A. Tzes, N. Koussoulas, and T. Stouraitis, "Efficient processor arrays for the implementation of generalised predictive-control algorithm," in *IEEE Proceedings - Control Theory and Applications*, 1998.

[50] L. G. Bleris, J. Garcia, M. V. Kothare, and M. G. Arnold, "Towards embedded model predictive control for system-on-a-chip applications," in *Journal of Process Control*, 2006.

[51] J. L. Jerez, P. J. Goulart, S. Richter, G. A. Constantinides, E. C. Kerrigan, and M. Morari, "Embedded Online Optimization for Model Predictive Control at Megahertz Rates," in *IEEE Transactions on Automatic Control*, vol. 59, 2014.

[52] M.-A. Boechat, J. Liu, H. Peyrl, A. Zanarini, and T. Besselmann, "An Architecture for Solving Quadratic Programs with the Fast Gradient Method on a Field Programmable Gate Array," in *MCCA*, 2013.

[53] E. N. Hartley and J. M. Maciejowski, "Predictive Control for Spacecraft Rendezvous in an Elliptical Orbit using an FPGA," in *ECC*, 2013.

[54] T. A. Johansen, W. Jackson, R. Schreiber, and P. Tondel, "Hardware architecture design for explicit model predictive control," in *ACC*, 2006.

[55] K. V. Ling, S. P. Yue, and J. M. Maciejowski, "A fpga implementation of model predictive control," in *ACC*, 2006.

[56] P. D. Vouzis, L. G. Bleris, M. G. Arnold, and M. V. Kothare, "A system-on-a-chip implementation for embedded real-time model predictive control," in *IEEE Transactions on Control Systems Technology*, 2009.

[57] D. Soudbakhsh and A. M. Annaswamy, "Parallel model predictive control," in *ACC*, 2013.

[58] B. Kapernick, S. Sub, E. Schubert, and K. Graichen, "A Synthesis Strategy for Nonlinear Model Predictive Controller on FPGA," in *UKACC International Conference on Control*, 2014.

[59] F. Xu, H. Chen, X. Gong, and Q. Mei, "Fast Nonlinear Model Predictive Control on FPGA Using Particle Swarm Optimization," in *IEEE Transactions on Industrial Electronics*, 2016.

[60] F. Xu, H. Chen, W. Jin, and Y. Xu, "FPGA Implementation of Nonlinear Model Predictive Control," in *CCDC*, 2014.

[61] H. Peyrl, H. Ferreau, and D. Kouzoupis, "A Hybrid Hardware Implementation for Nonlinear Model Predictive Control," in *IFAC*, 2015, pp. 87–93.

[62] B. Khusainov, E. C. Kerrigan, A. Suardi, and G. A. Constantinides, "Nonlinear predictive control on heterogeneous computing platform," in *IFAC*, 2017.

[63] M. Frigerio, J. Buchli, and D. G. Caldwell, "A domain specific language for kinematic models and fast implementations of robot dynamics algorithms," in *International Workshop on Domain-Specific Languages and Models for Robotic Systems*, 2015.

[64] C. A. Jara, F. A. Candelas, P. Gil, F. Torres, F. Esquembre, and S. Dormido, "Ejs+ejsrl: An interactive tool for industrial robots simulation, computer vision and remote operation," in *Robotics and Autonomous Systems*, 2011.

[65] M. Frigerio, J. Buchli, and D. G. Caldwell, "Code generation of algebraic quantities for robot controllers," in *International Conference on Intelligent Robots and Systems*, 2012.

[66] M. Bordignon, K. Stoy, and U. P. Schultz, "Generalized programming of modular robots through kinematic configurations," in *International Conference on Intelligent Robots and Systems*, 2011.

[67] J. Buch, J. Laursen, L. Sorensen, L. pEter Ellekilde, D. Kraft, U. Schultz, and H. Peterson, "Applying simulation and a domain-specific language for an adaptive action library," in *SIMPAR*, 2014.

[68] H. Kress-Gazit, G. E. Fainekos, and G. J. Pappas, "From structured english to robot motion," in *IROS*, 2007.

[69] H. Kress-Gazit, G. E. Fainekos, and G. J. Pappas, "A motion description language and a hybrid architecture for motion planning with nonholonomic robots," in *IROS*, 2007.

[70] E. Aertbelien and J. D. Schutter, "etasl/etc: A constraint-based task specification language and robot controller using expression graphs," in *International Conference on Intelligent Robots and Systems*, 2014.

[71] D. Vanthienen, M. Klotzbucher, J. D. Schutter, T. D. Laet, and H. Bruyninckx, "Rapid application development of constrained-based task modelling and execution using domain specific languages," in *International Conference on Intelligent Robots and Systems*, 2013.

[72] C. Finucane, G. Jing, and H. Kress-Gazit, "Ltlmop: Experimenting with language, temporal logic, and robot control," in *IROS*, 2010.

[73] U. Thomas, G. Hirzinger, B. Rumpe, C. Schulze, and A. Wortmann, "A new skill based robot programming language using uml/p statecharts," in *ICRA*, 2013.

[74] T. Kim and J. Yuh, "Task description language for underwater robots," in *IROS*, 2003.

[75] M. Morelli and M. D. Natale, "Control and scheduling co-design for a simulated quadcopter robot: A model-drivenapproach," in *SIMPAR*, 2014.

[76] N. Dantam, A. Hereid, A. Ames, and M. Stilman, "Correct software synthesis for stable speed-controlled robotic walking," in *RSS*, 2009.

[77] S. Longo, E. C. Kerrigan, K. V. Ling, and G. A. Constantinides, "Parallel move blocking model predictive control," in *CDC-ECC*, 2011.

[78] S. Kawakami, A. Iwanaga, and K. Inoue, "Many-core acceleration for model predictive control systems," in *Proceedings of the First International Workshop on Many-Core Embedded Systems*, 2013.

[79] P. Costa, A. Donnelly, A. Rowstron, and G. O'Shea, "Camdoop: Exploiting in-network aggregation for big data applications," in *USENIX Symposium on Networked Systems Design and Implementation*, 2012.

[80] L. Mai, L. Rupprecht, A. Alim, P. Costa, M. Migliavacca, P. Pietzuch, and A. L. Wolf, "Netagg: Using middleboxes for application-specific on-path aggregation in data centres," in *International Conference on Emerging Networking Experiments and Technologies*, 2013.

[81] M. Liu, L. Luo, J. Nelson, L. Ceze, A. Krishnamurthy, and K. Atreya, "Incbricks: Toward in-network computation with an in-network cache," in *International Conference on Architectural Support for Programming Languages and Operating Systems*, 2017.

[82] V. Jeyakumar, M. Alizadeh, Y. Geng, C. Kim, and D. Mazieres, "Millions of little minions: Using packets for low latency network programming and visibility," in *ACM Conference on SIGCOMM*, 2014.

[83] B. Schwartz, A. W. Jackson, W. T. Strayer, W. Zhou, R. D. Rockwell, and C. Partridge, "Smart packets: Applying active networks to network management," in *IEEE Second Conference on Open Architectures and Network Programming Proceedings*, 1999.